OFFICE OF NAVAL RESEARCH

Contract N00014-91-J-1927

R&T Code 413v001

Technical Report No. 11

SCANNING TUNNELING MICROSCOPY OF THE ORGANIC CONDUCTORS $(TMTSF)_2X$ ($X = CLO_4^-, ReO_4^-$)

by

SHULONG LI, HENRY S. WHITE & MICHAEL D. WARD

Prepared for Publication in the

JOURNAL OF THE AMERICAN CHEMICAL SOCIETY

University of Minnesota
Department of Chemical Engineering and Materials Science
Minneapolis, MN 55455

February 27, 1992

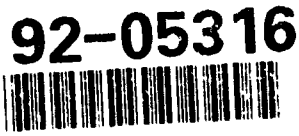

SECURITY CLASSIFICATION OF THIS PAGE

REPORT DOCUMENTATION PAGE

1a. REPORT SECURITY CLASSIFICATION **Unclassified**	1b. RESTRICTIVE MARKINGS
2a. SECURITY CLASSIFICATION AUTHORITY	3. DISTRIBUTION/AVAILABILITY OF REPORT **Unclassified/Unlimited**
2b. DECLASSIFICATION/DOWNGRADING SCHEDULE	
4. PERFORMING ORGANIZATION REPORT NUMBER(S) **ONR Technical Report 11**	5. MONITORING ORGANIZATION REPORT NUMBER(S)
6a. NAME OF PERFORMING ORGANIZATION **Dept of Chemical Engineering and Materials Science** 6b. OFFICE SYMBOL (*If applicable*) **Code 1113**	7a. NAME OF MONITORING ORGANIZATION **Office of Naval Research**
6c. ADDRESS (*City, State, and ZIP Code*) **University of Minnesota Minneapolis, MN 55455**	7b. ADDRESS (*City, State, and ZIP Code*) **800 North Quincy Street Arlington, VA 22217**
8a. NAME OF FUNDING/SPONSORING ORGANIZATION **Office of Naval Research** 8b. OFFICE SYMBOL (*If applicable*)	9. PROCUREMENT INSTRUMENT IDENTIFICATION NUMBER Contract No. N0001491-J-1927
8c. ADDRESS (*City, State, and ZIP Code*) **800 North Quincy Street Arlington, VA 22217-5000**	10. SOURCE OF FUNDING NUMBERS PROGRAM ELEMENT NO. / PROJECT NO. / TASK NO. / WORK UNIT ACCESSION NO

11. TITLE (*Include Security Classification*)
Scanning Tunneling Microscopy of the Organic Conductors $(TMTSF)_2X$ (X = ClO_4-, ReO_4-)

12. PERSONAL AUTHOR(S)
Shulong Li, Henry S. White and Michael D. Ward

13a. TYPE OF REPORT	13b. TIME COVERED	14. DATE OF REPORT (*Year, Month, Day*)	15. PAGE COUNT
Technical	FROM 1/1/91 TO 10/31/93	February 25, 1992	

16. SUPPLEMENTARY NOTATION
submitted to the J. Am. Chem. Soc.

17 COSATI CODES			18. SUBJECT TERMS (*Continue on reverse if necessary and identify by block number*)
FIELD	GROUP	SUB-GROUP	

19. ABSTRACT (*Continue on reverse if necessary and identify by block number*)
Scanning tunneling microscopy (STM) images of the (001) face (ab face) of the organic conductors $(TMTSF)_2X$ (TMTSF = tetramethyltetraselenafulvalene; X = ClO_4-) reflect the surface molecular corrugation and anisotropic stacking of TMTSF molecules along the [100] direction. The lattice constants of the (001) face determined from STM for $(TMTSF)_2ClO_4$ are a = 7.3 ± 0.2 Å, b = 7.8 0.2Å, and $\gamma = 69.5° \pm 2°$, and for $(TMTSF)_2ReO_4$ are 7.5 ± 0.2Å, b = 8.1 ± 0.2 Å, and $\gamma = 70° \pm 2°$, in excellent agreement with the known crystal structure. Height profile analysis of the tunneling current assigned to localized TMTSF electronic states are in agreement with the angle between the (001) face and the direction of the short axis of the TMTSF molecules. The STM images also are consistent with the high degree of electronic anisotropy of $(TMTSF)_2ClO_4$, with a broad electronic state density associated witht he psuedo one-dimensional TMTSF stacks and a highly localized state density associated with Se-Se contacts between stacks along the [110] direction. The results are corroborated by STM of isomorphous $(TMTSF)_2ReO_4$ which exhibits negligible tunneling current associated with the slightly larger Se-Se interstack distances in this compound. (cont)

20. DISTRIBUTION/AVAILABILITY OF ABSTRACT	21. ABSTRACT SECURITY CLASSIFICATION
☒ UNCLASSIFIED/UNLIMITED ☐ SAME AS RPT ☐ DTIC USERS	**Unclassified**
22a. NAME OF RESPONSIBLE INDIVIDUAL **Henry S. White**	22b. TELEPHONE (*Include Area Code*) (612) 625-6345 / 22c. OFFICE SYMBOL

DD FORM 1473, 84 MAR 83 APR edition may be used until exhausted
All other editions are obsolete

SECURITY CLASSIFICATION OF THIS PAGE

The lack of tunneling current in the interstack region of $(TMTSF)_2ReO_4$ signifies reduced electronic interaction transverse to the stacking direction, consistent with previously reported electronic properties of $(TMTSF)_2ReO_4$. The results indicate that STM can detect subtle differences in electronic structure that are responsible for bulk electronic properties.

Scanning Tunneling Microscopy of the Organic Conductors $(TMTSF)_2X$ ($X = ClO_4^-, ReO_4^-$)

Shulong Li, Henry S. White and Michael D. Ward*

Department of Chemical Engineering and Materials Science, University of Minnesota. Amundson Hall, 421 Washington Ave. SE, Minneapolis, MN 55455

Abstract

Scanning tunneling microscopy (STM) images of the (001) face (*ab* face) of the organic conductors $(TMTSF)_2X$ (TMTSF = tetramethyltetraselenafulvalene; $X = ClO_4^-, ReO_4^-$) reflect the surface molecular corrugation and anisotropic stacking of TMTSF molecules along the [100] direction. The lattice constants of the (001) face determined from STM for $(TMTSF)_2ClO_4$ are $a = 7.3 \pm 0.2$ Å, $b = 7.8 \pm 0.2$ Å, and $\gamma = 69.5^o \pm 2^o$, and for $(TMTSF)_2ReO_4$ are 7.5 ± 0.2 Å, $b = 8.1 \pm 0.2$ Å, and $\gamma = 70^o \pm 2^o$, in excellent agreement with the known crystal structure. Height profile analysis of the tunneling current assigned to localized TMTSF electronic states are in agreement with the angle between the (001) face and the direction of the short axis of the TMTSF molecules. The STM images also are consistent with the high degree of electronic anisotropy of $(TMTSF)_2ClO_4$, with a broad electronic state density associated with the psuedo one-dimensional TMTSF stacks and a highly localized state density associated with Se-Se contacts between stacks along the [110] direction. The results are corroborated by STM of isomorphous $(TMTSF)_2ReO_4$ which exhibits negligible tunneling current associated with the Se-Se states, in agreement with the slightly larger Se-Se interstack distances in this compound. The lack of tunneling current in the interstack region of $(TMTSF)_2ReO_4$ signifies reduced electronic interaction transverse to the stacking direction, consistent with previously reported electronic properties of $(TMTSF)_2ReO_4$. The results indicate that STM can detect subtle differences in electronic structure that are responsible for bulk electronic properties.

---

*Author to whom correspondence should be addressed

Introduction

Molecular crystalline solids based on organic and organometallic components numerous electronic phenomena, including electrical conductivity, superconductivity, non-linear optical behavior and ferromagnetism.[1] The most extensively examined molecular crystals have been the low-dimensional conductors, which generally exhibit anisotropic conductivity along axes containing stacks of open-shell charge transfer molecules that are responsible for the formation of extended band structure. Most notable among these are the organic superconductors.[2] While the superconductivity critical temperatures are lower than those of oxide superconductors[3] or the more recently discovered superconducting phases of alkali-doped C_{60},[4] these materials present an opportunity to examine structure-function relationships of extended solids.

The principle advantage of molecular materials is the ability to rationally control bulk properties through molecular design. This requires, however, a more thorough understanding of the relationship between molecular structure, supramolecular structure and electronic properties coupled with engineering of intermolecular interactions in the solid state. There is also a need to better understand the crystal growth of these materials on a molecular level in order to better control size, morphology, growth orientation, selectivity (towards different polymorphs) and defect structure. In particular, the electrochemical crystal growth method commonly employed for the synthesis of low-dimensional organic conductors is still not well understood. Further advances in the synthesis of new molecular materials, therefore, will require microscopic-level understanding of the *surface* topography and electronic structures as well as those of the bulk. The capabilities provided by scanning tunneling microscopy (STM)[5] and atomic force microscopy (AFM)[6] have encouraged us to examine molecular crystals with these methods.

The tunneling current, i_T, measured in STM is proportional to the density of states (DOS), or $\rho(r,E_F)$, at a position r above the surface and at the Fermi energy, E_F.[7,8] Operation of the STM with a constant applied current between the tip and the substrate forces the tip height to vary in order to maintain a constant $\rho(r,E_F)$ as the tip is scanned across the surface. Conversely, when the

vertical position of the tip is fixed, variation in i_T is measured that reflects the spatial dependence of $\rho(r,E_F)$. In either mode, the contrast observed in STM images (variations in r in constant current operation or i_T in constant height operation) reflects both the surface topography as well as the local surface density of states (LDOS). Although the tunneling current decays exponentially with distance of the tip from states on the surface of the sample, it is possible that surface regions closer to the tip but with small LDOS will afford minimal tunneling current, and vice-versa. Accurate separation of topographical and electronic contributions is especially important when examining molecular crystals which typically are not atomically flat, but rather have atoms and portions of molecules protruding from an average surface plane. In this case, the tunneling current will depend on the molecular corrugation *and* LDOS of the molecular constituents in the crystal plane. When interpreting STM images of molecular conductors it is reasonable to invoke the tight-binding approximation,[9] in which the states near the Fermi energy are assumed to comprise linear combinations of the highest occupied molecular orbital (HOMO) or the lowest unoccupied molecular orbital (LUMO) on the constituent molecules. Of particular interest is whether STM images of molecular crystals can be interpreted on this basis, and whether the measured LDOS can be correlated with the bulk electronic structure.

One of the more extensively investigated series of organic conductors has been the mixed-valence $(TMTSF)_2X$ salts,[10] many of which are superconducting at very low temperatures. Very subtle changes in composition and structure, however, can result in rather dramatic changes in electronic properties. For example, $(TMTSF)_2ClO_4$ is superconducting near 1 K at ambient pressure,[11] but the isomorphous $(TMTSF)_2ReO_4$ exhibits a sharp metal-insulator (M-I) transition at 182 K[12] and only becomes superconducting at 1.3 K at pressures exceeding 9.5 kbar.[13] A M-I transition has also been observed for the isostructural $(TMTSF)_2PF_6$ at 12 K,[14] and superconductivity is only observed at 0.9K at pressures exceeding 12 kbar.[15] The observations of M-I transitions in the ReO_4^- and PF_6^- salts can be attributed to a reduction in the transfer integrals transverse to the one-dimensional stacking axes that results from increases in the interstack Se-Se

distances.[16] These striking differences in electronic properties prompted us to investigate the local electronic structure of $(TMTSF)_2ClO_4$ and $(TMTSF)_2ReO_4$ using STM.

Recently, STM has been used to examine several low-dimensional inorganic conductors[17] and superconductors,[18] as well as organic solids, including bis(ethylenedithiotetrathiafulvalene) salts,[19] tetrathiafulvalenium-tetracyanoquinodimethanide,[20] and other tetracyanoquinodimethanide salts.[21] Low-temperature tunneling spectroscopy[22] of organic superconductors, including point-contact studies, to determine the BCS superconducting gap also has been examined with STM.[23] A recent STM study of $(TMTSF)_2ClO_4$ and $(TMTSF)_2PF_6$ reported similar images for both salts,[24] but details about the DOS were limited by the relatively poor quality of the STM data. Localized "spherical" regions of high tunneling current were attributed to ClO_4^- anions, although these closed shell anions would not be expected to have states near E_F to contribute to the tunneling current. We present herein STM studies of the isomorphous $(TMTSF)_2ClO_4$ and $(TMTSF)_2ReO_4$ that reveal clearly the LDOS associated with the one-dimensional TMTSF stacks responsible for the anisotropic conductivity of these materials. The STM images are in excellent agreement with the reported crystal structures and can be interpreted on the basis of the TMTSF molecular orbitals. Significantly, the STM images of $(TMTSF)_2ClO_4$ reveal interstack Se-Se contacts which are absent in $(TMTSF)_2ReO_4$. This observation is attributed to the reduction in the bandwidth transverse to the stacking axis in the latter that is manifested in its M-I transition. The data indicate that STM can be used to probe macroscopic electronic behavior on a molecular level in low-dimensional molecular solids.

Experimental

Crystals of $(TMTSF)_2ClO_4$ and $(TMTSF)_2ReO_4$ were grown by electrochemical oxidation of TMTSF (Aldrich) on a platinum wire (1 cm length x 0.0127 cm diameter) at a current density of 4.7 mA cm^{-2} in methylene chloride containing 1.0 x 10^{-3} M TMTSF and 0.1 M n-$Bu_4N^+ClO_4^-$ or n-$Bu_4N^+ReO_4^-$. This process typically yielded 3-6 long, flat single crystals with typical crystal

dimensions of 4 x 0.5 x 0.05 mm (Figure 1). The (001) face of $(TMTSF)_2ClO_4$ was larger than the (001) face of $(TMTSF)_2ReO_4$ signifying to slower growth along the *b* direction in the latter.

A Nanoscope II ™ scanning tunneling microscope with mechanically cut 80% Pt/20% Ir or 70% Pt/30% Rh tips was used to obtain images. Crystals were mounted onto an aluminum substrate that provided electrical conduction to the STM fixture. All crystals were rinsed with neat methylene chloride prior to mounting and image acquisition. Images of both $(TMTSF)_2ClO_4$ and $(TMTSF)_2ReO_4$ were obtained in either constant height or constant current mode, although the images shown here were obtained at constant height as slightly better resolution was obtained under these conditions. Bias voltages ranging from +400 to -400 mV (tip vs. sample) were employed, with high quality images obtained with either polarity. Set point currents ranged from 0.5 - 1.5 nA. Generally, higher set point currents and lower bias voltages gave better STM images. Extended Huckel calculations were performed at the STO-3G level using a Tetronix CACHE molecular modeling workstation. Image analyses were performed on a Macintosh IIcx personal computer using Image, a public domain image analysis program available from National Center for Supercomputing Applications (University of Illinois Urbana-Champaign).

Results and Discussion

Crystal structure and crystal plane topography. The isomorphous mixed-valence salts $(TMTSF)_2ClO_4$ and $(TMTSF)_2ReO_4$ crystallize in the $P\bar{1}$ space group. The lattice constants of the two compounds are similar, although *b* and *c* are 0.95 % and 1.6 % larger, respectively, in $(TMTSF)_2ReO_4$ (Table 1). Both structures exhibit psuedo one-dimensional stacks of TMTSF molecules stacked along the *a* axis in a "zig-zag" motif, with the stacks forming "sheets" along the *b* axis (Figure 1). These sheets occupy the *ab* (001) plane, which is depicted in the left panel of Figure 1. The center panel depicts the view normal to the *bc* plane, where these sheets are readily evident. The orientation of the (001) plane is also shown as the dark line at the bottom of the center panel, with this plane projecting normal to the plane of the paper. The short axis of the TMTSF molecules is tilted by 32° with respect to the (001) plane, given by the angle Ω in Figure

1. The anions, which reside in "pockets" created by the zig-zag motif, are disordered at 295 K in two different orientations as required by the space group symmetry, each orientation having equal occupancy.

A very slight dimerization of the TMTSF stacks along the *a* axis is evident from the crystal structure, which reveals two crystallographically independent distances between planes of neighboring TMTSF molecules. This dimerization is accompanied by the formation of a small gap at the Brillouin zone boundary, but the uppermost band is still one-half filled and metallic behavior still operative in both materials at room temperature. The ReO_4^- salt, however, exhibits a metal-insulator transition at 182 K, which has been attributed to a Peierls transition induced by coupling to anion ordering.[10] This conclusion was based on greater interaction between the ReO_4^- anions and TMTSF sites as surmised from the shorter TMTSF-O distances in the crystal structure. In addition, the shortest interstack Se-Se distances in $(TMTSF)_2ReO_4$ (3.827 Å) is greater than that in $(TMTSF)_2ClO_4$ (3.778 Å). The distance between Se atoms in the latter is therefore less than the sum of the van der Waals radii of the two selenium atoms (3.80 Å[25]), whereas this distance is slightly greater than the sum of the van der Waals radii in the former. This suggests that the electronic interaction between Se atoms will be significantly different in the two salts. Indeed, interstack Se-Se overlap mitigates against metal-insulator phase transitions and is an important determinant of electronic band structure and properties.[26]

The observed morphology of the crystals is consistent with the x-ray crystal structure as deduced from the expected interactions between molecules along the different crystallographic directions during crystal growth. Crystal morphology is dictated by the rate of growth along different directions, with the largest faces normal the slowest growth direction. In these materials, the fastest growth rate is along the [100] direction (*a* axis), which can be attributed to the high conductivity along this directions and to strong π–π interactions between TMTSF molecules. The next fastest growth rate is along the [010] direction (*b* axis) due to sigificant, but weaker, Se-Se interactions between adjacent TMTSF stacks. Notably, we have observed that the growth rate along the [010] direction, relative to [100], is slower for the $(TMTSF)_2ReO_4$, suggesting weaker

interstack interactions in this material (this point is important for the discussion of STM images to follow). Finally, slow growth along the [001] (*c* axis) in both salts can be attributed to very weak interstack interactions between the anions and the methyl groups of the polarizable cations (with an average charge of only 0.5+ per TMTSF molecule). Hence, the largest crystal face is the *ab* (001) face, which contains the (001) plane with the long axis of the crystal parallel to the stacking *a* axis. Because the geometric surface areas of the (010) and (100) faces are extremely small we restricted our investigations to the (001) face. The STM tip, shown below this plane in the center panel of Figure 1, is therefore scanned over the TMTSF sheets in the (001) plane.

[Figure 1]

STM images of $(TMTSF)_2ClO_4$. STM images of the (001) face of $(TMTSF)_2ClO_4$ typically exhibited large, defect free, molecularly flat regions. These images of the (001) face exhibited a tunneling current corrugation along the *a* axis with large bright features (A) having dimensions of approximately 3 Å x 6 Å (Figure 2). These features are separated by dark regions (B). A second bright, but smaller, feature (C) is also evident, alternating with a dark region (D) along the *a* axis. The observed tunneling current topography is consistent with adjacent stacks of TMTSF molecules aligned along the *a* axis. The average periodicity measured from line profiles of the tunneling current gave $a = 7.3 \pm 0.2$ Å and $b = 7.8 \pm 0.2$ Å,[27] in good agreement with the corresponding lattice parameters determined by x-ray crystallography (Table 1). The angle between these two directions was $69.5^{o} \pm 2^{o}$, in reasonable agreement with $\gamma = 70.43^{o}$ determined crystallographically.

[Figure 2]

Extended Huckel calculations indicate that the TMTSF HOMO (which becomes the partially occupied molecular orbital, or POMO, in the partially oxidized $TMTSF^{0.5+}$ molecules in the mixed

valence salts) consists largely of in-phase contributions from Se atoms, with small contributions from the ring C=C bonds. The LUMO has large out-of-phase contributions from the ring C=C bonds. The average degree of oxidation per TMTSF site ($\rho = 0.5+$) is tantamount to states that are 3/4-filled, equivalent with 3 electrons per two TMTSF sites. Consequently, the tight-binding band structure results from linear combinations of the 3/4-filled POMO, or equivalently, from combination of an equal number of filled ($2e^-$/site) and half-filled ($1e^-$/site) TMTSF POMOs. The slight $4k_F$ dimerization evident from the x-ray crystal structure that leads to small gap at the Brillouin zone boundary results in a lifting of the degeneracy of the molecular orbitals of the TMTSF sites. The loss of degeneracy results in a 1/2 filled orbital; therefore, the uppermost band in the tight-binding description is 1/2-filled and the $4k_F$ gap is not at the Fermi level. This is represented in Scheme I, which depicts the evolution of the tight-binding band structure from the TMTSF POMO (denoted here simply as ○). In particular, Scheme I depicts the states at the bottom, center and top of the two bands, and their phase relationships. The lower band is filled and is not expected to contribute significantly to the tunneling current. The upper band, however, is half-filled, the Fermi level positioned at the center of this band. The absence of a gap at the Fermi level is consistent with our observation of identical images for bias voltages of either polarity, which indicates metallic behavior attributable to a 1/2-filled conduction band. Tunneling via states in the conduction band near this Fermi level therefore is expected to dominate the STM data.

Scheme I

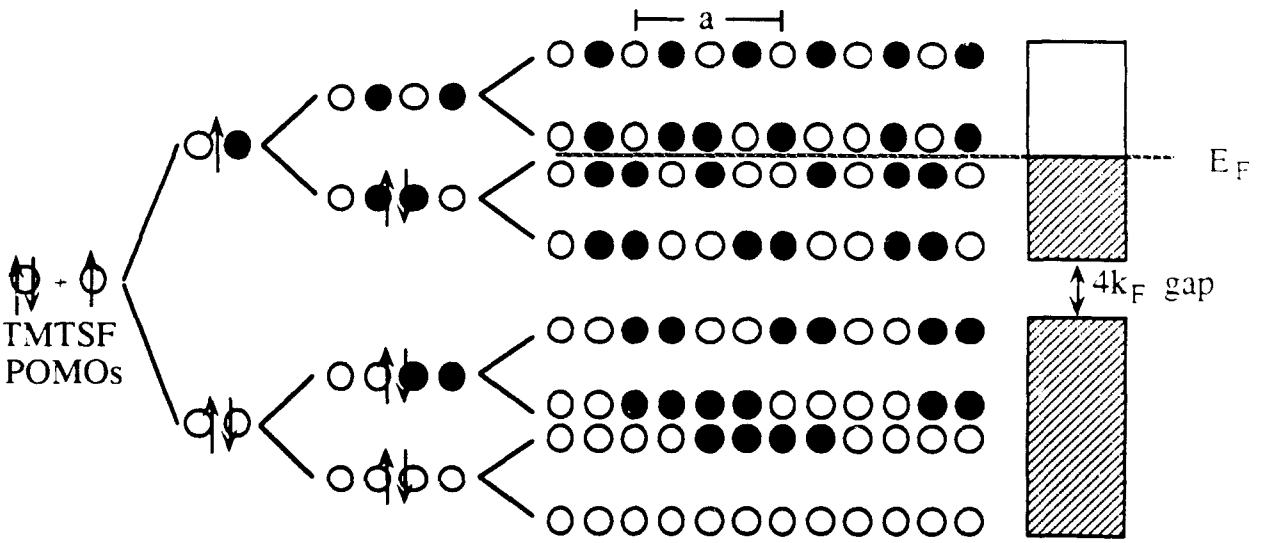

If the molecular motif of the (001) plane is overlaid on the STM image, there are several interpretations that appear to provide commensurate registration of the image contrast and the molecular structure of the (001) plane. The six most reasonable interpretations are depicted in Figure 3, in which the TMTSF molecules are represented as rectangles and the anions as overlapping cross-hatched squares (describing the disordered pair of tetrahedral anions). Inspection of the crystal structure reveals that Se-Se distances between Se atoms along approximately[28]the [110] direction (the bisector of the *ab* axes) of 3.778, 3.865 and 3.955 Å, compared to the Se-Se distances of 4.192, 5.279 and 5.314 Å along the [010] direction. The Se-Se contacts are evident from the space-filling models in Figure 4. The TMTSF "rectangles" in Figure 3 indicate the close contact along the [110] direction with signficantly less contact along the [010] direction (*b* axis). Space-filling representations of the (001) face shown in Figure 4 are also helpful when interpreting the STM images. The models on the left depict the (001) face terminated with TMTSF molecules while the models on the right are terminated with ClO_4^- anions, which are portrayed with both halves of the disordered pair.

The following discussion of the interpretation of the STM image, based on the six possible structures shown in Figure 3, considers termination of the (001) face with either TMTSF molecules or ClO_4^- anions. In all cases corrugation of the tunneling current is expected.

[Figure 3]

[Figure 4]

1. The (001) face terminated with TMTSF molecules.

(a) Region A corresponds to LDOS associated with every other TMTSF molecule along the one-dimensional stack. The corrugation of tunneling current, which results from changes in $\rho(r,E_F)$, must correspond to either corrugation of the electronic states or the molecular corrugation of the *ab* plane in which the TMTSF molecules alternate in a zig-zag manner (Figure 4, left). The width and length of this feature are essentially the same as the molecular thickness of the TMTSF molecule (ca. 3.5 Å) and molecular width resolved in the (001) plane, respectively. Region A therefore corresponds to tunneling to states on the TMTSF molecules protruding from the *ab* plane and region B the TMTSF molecules that are recessed in the *ab* plane. Region C overlays the Se-Se interstack contacts that are responsible for the formation of electronic states between stacks along the [110] direction. The negligible amount of state density observed in region D can be attributed to smaller Se-Se interactions resulting from larger Se-Se distances along the [010] direction, consistent with the crystal structure. The tunneling current within region A decreases monotonically along the [010] direction (proceeding left to right across the feature in this region). The angle between this profile and the (001) plane is $37^o \pm 6^o$, as measured from topographical line profile analysis. This value is in reasonable agreement with the 32^o angle between the (001) plane and the short axis of the TMTSF molecules (see Figure 2). Notably, the POMO of TMTSF, based on contributions from the Se atoms and C=C region, is oriented along the short axis of the TMTSF molecule.

This strongly suggests that the observed tunneling contrast corresponds to the local molecular orbitals on TMTSF molecules.

(b) The large tunneling current in region A corresponds to LDOS associated with Se-Se contacts between stacks along the [110] direction. The more localized tunneling current in region C would then be attributed to the region of overlap between the TMTSF POMOs, but only between every other pair of TMTSF molecules. The absence of tunneling current in region B therefore implies negligible tunneling to the one-half of the regions between the TMTSF molecules. Inspection of the crystal structure, however, does not indicate any structural basis for this behavior. The absence of tunneling current in region D is consistent with the absence of states along the [010] direction due to the negligible Se-Se interactions.

(c) The large tunneling current in Region A corresponds to LDOS associated with mixing of the TMTSF POMOs between every other pair of TMTSF molecules, resulting in tunneling current on every other $(TMTSF)_2^+$ dimer. Accordingly, the absence of tunneling current in region B would imply negligible DOS between one-half of the TMTSF molecules. The width of the feature in region A is near that expected for the 3.3 Å separation between planes. The state density in region C may be attributed to electronic states formed by Se-Se interactions between stacks along the [110] direction. The absence of tunneling current in region D is consistent with the absence of states along the [010] direction due to the negligible Se-Se interactions.

II. The (001) face terminated with ClO_4^- anions.

(d) The anions occupy the dark regions B where they obscure every other TMTSF molecule in a given stack, their lack of states at the Fermi level inhibiting the tunneling current. Region A results from tunneling to LDOS associated with TMTSF molecules that are not blocked by the anions (Figure 4, right). Since the anion rests in "pockets" formed by TMTSF molecules that are recessed in the *ab* plane, the height of the exposed TMTSF molecules is < 2 Å below that of the anion. Tunneling to these molecules, however, is feasible because of their high density of states at E_F compared to the anions. The exposed TMTSF molecules are offset by

a/2 with respect to the adjacent stack, identical to the pattern of tunneling current observed in the STM image.

It should noted that the space filling models in Figure 4 portray the anions in both disordered, equal occupancy positions. Notably, the shapes of the local tunneling features are constant in the areas imaged. If the disorder was static and both positions were present and randomly disordered, or if the disorder was dynamic on a time scale slower than image acquistion, we expect that the tunneling features would vary in the imaged area. The constancy of the tunneling features therefore suggests either the presence of one set of the half-occupancy *statically* disordered anions, or alternatively, anion disorder that is dynamic on a time scale faster than that of image acquisition. The state density in region C may be attributed to electronic states formed by Se-Se interactions between stacks along the [110] direction. The negligible tunneling current in region D can be attributed to smaller Se-Se interactions along the [010] direction. The monotonic decrease in tunneling current within region A along the [010] direction as described in (a) is consistent with the orientation of the short axis of the TMTSF molecules.

(e) Region A corresponds to LDOS associated with Se-Se interstack contacts along the [110] direction. Negligible tunneling current in region D corresponds to weak Se-Se interactions along the [010] direction. The tunneling current observed in region C is attributed to LDOS on the anions. In this interpretation tunneling to the TMTSF molecules exposed at the surface is not operative.

(f) The large tunneling current in region A is associated with the anions, which are closest to the tip as its scans the surface of the *ab* plane. No tunneling current is observed in region B, in which the exposed TMTSF molecules reside.

Consideration of the properties of the molecular constituents of $(TMTSF)_2ClO_4$ and its crystal structure enables elimination of some of the above alternatives. Unlike the $TMTSF^{0.5+}$ molecules, the closed shell anions are not expected to have appreciable local state density at the

Fermi level and therefore should not correspond to local regions of high tunneling current. We also note that the reversible reduction potential for the $TMTSF^{o/+}$ couple is 0.42 V (vs. SCE)[29] while the ClO_4^- anion is electrochemically inert at least in the range $2.5 > E > -2.5$ V. Accordingly, (e) and (f), which both invoke tunneling into regions occupied by the anions, are considered unlikely. The high conductivity anisotropy measured for $(TMTSF)ClO_4$ can be attributed to a highly anisotropic electronic band structure in which the electronic states near the Fermi energy primarily result from coupling between TMTSF molecules in the stacking directions, with relatively small contributions from interstack coupling. The transfer integral of the structurally similar $(TMTSF)_2PF_6$ is approximately 0.25 eV but the transverse transfer integral is approximately 0.003 eV.[30] Alternative (b) therefore seems unlikely because it suggests a larger density of states between stacks than within stacks. In addition, our STM investigations of $(TMTSF)_2ReO_4$ support the assignment of the tunneling features in Region C to Se-Se interactions (vide infra).

The distances between the STM tip and all TMTSF interplanar regions are essentially identical. Therefore, the attribution of highly localized tunneling current to states on every other dimer according to the description in (c) would require a corresponding electronic state localization in the TMTSF stacks on the surface plane. Interestingly, the Fermi level of $(TMTSF)_2ClO_4$ is located in the center of the conduction band which, according to the tight binding approximation, consists of states having in-phase combinations resembling $(TMTSF)_2$ dimers repeating at periods of a, separated by $a/2$ (Scheme I). The electronic structure of the tight-binding wavefunctions at E_F therefore is topologically similar to the corrugation of the tunneling current in a given stack, suggesting a possible electronic basis for the observed tunneling current contrast. However, the tunneling features on the (001) face are offset in adjacent stacks by $a/2$, which would imply strong coupling between stacks. This modulation of tunneling current between adjacent stacks resembles a commensurate charge-density wave (CDW) with anti-phase modulation,[31] which signifies significant Coulombic interaction between TMTSF stacks resulting from charge localization. This ordered CDW state, however, is not consistent with metallic conductivity of $(TMTSF)_2ClO_4$ or

with the very slight dimerization of the TMTSF stacks. We also note that other $2k_F$ CDW instabilities have not been observed in $(TMTSF)_2ClO_4$.[32] It is feasible that the lack of centrosymmetry and absence of ClO_4^- anions on the outer surface layer of TMTSF molecules could provide local anisotropic potential fields in the surface plane and a CDW-like state, thereby inducing charge pinning on the surface layer (in this case, the STM image would actually correspond to surface CDW states instead of states associated with the electronic structure of the bulk solid). Coulombic interactions and anisotopic potential fields that induce structural and electronic distortions have been noted for one-dimensional platinum chain compounds.[33] However, this assignment of the tunneling current contrast to either bulk or surface CDWs is not supported by the observation that current of the opposite polarity produced identical images. Based on this observation and the inconsistency between an anti-phase modulated CDW and its implicit charge localization and the known electronic properties of $(TMTSF)_2ClO_4$, we conclude that a structural basis for the observed tunneling current contrast is more likely than one solely based on electronic states.

If electronic considerations alone were considered in alternative (a) the observed tunneling current would imply a dramatic charge localization in a manner reminscent of a "monovalent" electronic structure (...$A^+A^oA^+A^o$...),[34,35] but this also would not be consistent with the observed metallic conductivity and polarity independent images. The molecular corrugation of the *ab* face, however, is qualitatively consistent with alternative (a). Within a given stack the height of the TMTSF molecules with respect to the tip alternate in a zig-zag fashion with a corrugation of approximately 1.7 Å. This motif is repeated in an adjacent stack but translated by *a*/2. The sensitive dependence of the tunneling current on the distance between the POMO and the STM tip is therefore manifested in the observed topology of $\rho(r,E_F)$. We note, however, that height profiles of the tunneling current along the stacking direction are consistent with a corrugation of > 6 Å, far exceeding the molecular corrugation based on the crystal structure. Images acquired at higher bias voltages still indicated a total absence of tunneling current in region B. It therefore

seems reasonable to suggest that the relatively small molecular corrugation on the (001) face is not responsible for the observed image contrast.

Based on the above arguments, we favor an interpretation of the STM image in which a (001) face covered with anions (Figure 4, right) as described in (d). It is reasonable to suggest negligible DOS near the Fermi level on the closed shell anions which would result in blocking of tunneling current to the TMTSF molecules beneath the anions. The molecular structure of the (001) plane covered with ClO_4^- anions and tunneling current corrugation are topologically similar. That is, the TMTSF molecules that are "exposed" on the (001) plane have states accessible to the STM tip; these exposed TMTSF molecules repeat at intervals of a with a separation of $a/2$, and are offset by $a/2$ with respect to adjacent stacks, in agreement with the tunneling current contrast. It is especially important to reiterate the agreement between the value of the angle between the short axis of the TMTSF molecules and the (001) plane as measured in our STM studies and as measured from the x-ray crystal structure. Since the TMTSF POMO is oriented along the short axis, this demonstrates that the tunneling current accurately reflects the molecular wavefunctions on the TMTSF sites.

In summary, (1) an anti-phase modulated CDW state with charge pinning is inconsistent with the metallic conductivity of $(TMTSF)_2ClO_4$ and the polarity independent images, (2) the corrugation of TMTSF molecules on the (001) plane is significantly smaller than that indicated by the tunneling current corrugation and (3) tunneling to anion states is not likely since these species do not have a significant DOS at the Fermi level. We therefore conclude that alternative (d) is the most reasonable interpreation of the observed STM data.

STM images of $(TMTSF)_2ReO_4$. Images of the *ab* plane of $(TMTSF)_2ReO_4$ were similar to those of the $(TMTSF)_2ClO_4$ (Figure 2a). The lattice constants determined by STM were $a = 7.5 \pm 0.2$ Å, $b = 8.1 \pm 0.3$ Å and $\gamma = 70^o \pm 2^o$. The larger values of a and b are consistent with the differences observed in the single-crystal structures of the two salts. The large features along the a axis are attributed to tunneling into sites on the TMTSF stacks. The resemblance between the two

images suggests that the images shown here for $(TMTSF)_2ClO_4$ and $(TMTSF)_2ReO_4$ represent crystal planes with identical molecular motifs. *Images of $(TMTSF)_2ReO_4$, however, exhibit substantially reduced tunneling current in region C compared to $(TMTSF)_2ClO_4$.* Grayscale histograms recorded along a 5 Å wide band coincident with the [110] direction clearly demonstrate the smaller tunneling current in region C for the $(TMTSF)_2ReO_4$ (Figure 5).

We attribute the difference in the LDOS in region C to the difference in electronic anisotropy of these two materials. In order for tunneling to occur to a local state the width of the band comprising the local wavefunctions must be large enough to obviate electron localization, and the energy band must cross at or near the Fermi level. As described above, while the differences in the *a* lattice parameter are negligible, the *b* and *c* lattice parameters are larger for $(TMTSF)_2ReO_4$, resulting in longer Se-Se interstack contacts for this salt. Notably, superconductivity is observed at 1K under ambient pressure for $(TMTSF)_2ClO_4$, but $(TMTSF)_2ReO_4$ exhibits a M-I transition at 182 K and superconductivity only under an applied pressure. The M-I transition is suppressed by pressure due to compression of the lattice. The single crystal x-ray structures and electronic properties are consistent with a smaller transfer integral and correspondingly smaller bandwidth along the transverse direction for the ReO_4^- salt; i.e., more electron localization within the TMTSF stack and less electronic interaction between stacks. This is equivalent to stating that the band structure of the ReO_4^- salts is more anisotropic than that of the ClO_4^- salt, i.e., the dimensionality of the band structure is lower in the former. The higher dimensionality and the more circular Fermi surface of the ClO_4^- salts inhibits the metal-insulator transition because the bandgap associated with the Peierls distortion is not formed everywhere on the Fermi surface.

The importance of two-dimensional metallic character provided by interstack interactions in suppressing phase transitions and obtaining superconducting behavior in organic metals has been demonstrated for bis(ethylenedithiotetrathiafulvalene) salts, in which interstack S-S interactions result in transverse band structure.[36] The small transverse transfer integral in the TMTSF salts (t = 0.003 eV for the analogous $(TMTSF)_2PF_6$[37]) suggests that the electronic properties and tendency

towards phase transitions would be very sensitive to small changes in the interstack Se-Se distances. The notable absence of tunneling current at the Se-Se sites in the STM images of $(TMTSF)_2ReO_4$ therefore is attributed the decrease in bandwidth and a corresponding lowering of the conductivity of the band based on the overlap of the Se wavefunctions transverse to stacking axis. The macroscopic electrical properties of these two salts are therefore a manifestation of the local electronic structure observed in these STM images. Notably, the different tunneling characteristics of the two salts in region C also corroborates the assignment of these features in region C to Se-Se contacts that give rise to electronic band structure in the transverse direction in the ClO_4^- salt. This finding is also consistent with the observation that growth along the [010] direction is considerably slower for $(TMTSF)_2ReO_4$ crystals than for $(TMTSF)_2ClO_4$, due to smaller intermolecular Se-Se interactions transverse to the one-dimensional stacking axis in the former material.

[Figure 5]

Conclusions

The (001) *ab* planes of $(TMTSF)_2ClO_4$ and $(TMTSF)_2ReO_4$ can be imaged using STM with molecular-scale resolution, providing details of the crystallographic and electronic structure of these materials. The STM images are consistent with the known crystal structures and the presence of TMTSF stacks, as well as the molecular orientation on the (001) plane. The observation of significant tunneling current in the region of Se-Se interstack contacts in $(TMTSF)_2ClO_4$ and the absence of these features in $(TMTSF)_2ReO_4$ corresponds to a smaller transfer integral and bandwidth transverse to the stacking direction in the latter. This property is manifested in the metal-insulator transition at 182 K observed previously for $(TMTSF)_2ReO_4$. In this case, the STM has provided a correlation between surface DOS and macroscopic electronic properties as well as molecular-level characterization of the physical and electronic structure of crystal surfaces. The ability to obtain clear images of different crystal planes may provide insight into the

electrocrystallization process, in particular the relationship between electron transfer at different crystal planes and crystal morphology. In addition, detailed understanding of the surface molecular and electronic structure may provide a basis for nanoscale STM assisted molecular synthesis on single crystals of these materials.

Acknowledgments. The support of the National Science Foundation (Grant NSF/DMR-9107179), the Office of Naval Research and the Center for Interfacial Engineering (NSF Engineering Research Centers Program, CDR 8721551) is gratefully acknowledged.

Table I. Lattice constants for $(TMTSF)_2ClO_4$ and $(TMTSF)_2ReO_4$ as determined from the single crystal x-ray crystal structure collected at 295 K.[16]

Compound	a (Å)	b(Å)	c(Å)	α	β	γ	V(Å^3)
$(TMTSF)_2ClO_4$	7.266	7.678	13.27	84.58	86.73	70.43	694.4
$(TMTSF)_2ReO_4$	7.284	7.751	13.483	83.23	86.56	70.08	710.5

Figure Captions

Figure 1. Crystal structure of $(TMTSF)_2ClO_4$ as viewed normal to the *ac* plane (left), normal to the *bc* plane (center) and normal to the *ab* plane (right). The *ab* (001) plane, illustrated as a dark line below the *bc* plane in the center panel, projects normal from the plane of the paper. The STM images were acquired on the *ab* face; the STM tip depicted in the figure therefore is normal to the *ab* face and is scanned left-to-right right and normal to the plane of the paper with respect to the center panel. A schematic representation of electrochemically grown $(TMTSF)_2X$ crystals is also illustrated.

Figure 2. (a) STM image of (a) the *ab* face $(TMTSF)_2ClO_4$ and (b) the *ab* of $(TMTSF)_2ReO_4$. Conditions: constant height mode, tip bias = +90 mV; setpoint current = 1.3 nA. Regions A-D are described in the text. Maximum contrast corresponds to 11 Å in (a) and (b).

Figure 3. Six alternative correlations between the crystal structure and the tunneling current in STM images of $(TMTSF)_2ClO_4$. Detailed explanations are given in the text. The cross-hatched disordered squares represent the ClO_4^- anions and the rectangular bars the TMTSF molecules.

Figure 4. Space filling representations viewed along the *ab* plane (upper left) and normal to the *ab* plane (lower left) for $(TMTSF)_2ClO_4$ with the *ab* plane terminated with TMTSF molecules, and along the *ab* plane (upper right) and normal to the *ab* plane (lower right) when the *ab* plane is terminated with ClO_4^- molecules. The Se atoms are shaded white and the ClO_4^- anions are represented as their disordered pairs.

Figure 5. (b) Grayscale histograms along a band coincident with the [110] direction for $(TMTSF)_2ClO_4$ (upper) and $(TMTSF)_2ReO_4$ (lower). The unshaded areas indicate the DOS in region A, whereas the shaded areas indicate the state density in region C associated with Se-Se states. The fine structure in the histograms is not reproducible and therefore does not correspond to any meaningful interpretation.

[1](a) Lehn, J.-M. *Angew. Chem. Int. Ed. Eng.* **1988**, *27*, 89. (b) *Molecular Electronic Devices*, Carter, Forrest L., Ed.; Marcel Dekker, New York, **1982**. (c) *Extended Linear Chain Compounds*, Vol 1 - 3, Miller. J.S., Ed.; Plenum, New York, **1982-1983**. (d) Desiraju, G. Crystal Engineering, Elsevier, New York, 1989. (e) Miller, J. S.; Epstein, A. J.; Reiff, W. M. *Science*, **1988**, *240*, 40.

[2](a) Williams, J. M.; Carneiro, K. *Adv. Inorg. Chem. RadioChem.*, **1985**, *29*, 249. (b) Inokuchi, H. *Angew. Chem. Int. Ed. Eng.* 1988, 27, 1747-1751. (c) Emge, T. J.; Leung, P. C. W.; Beno, M. A.; Wang, H. H.; Firestone, M. A.; Webb, K. S.; Carlson, K. D.; Williams, J. M.; Venturini, E. L.; Azevedo, L. J.; Schirber, J. E. *Mol. Cryst. Liq. Cryst.* **1986**, *132*, 363. (d) Montgomery, L. K.; Geiser, U.; Wang, H. H.; Beno, M. A.; Schultz, A. J.; Kini, A. M.; Carlson, K. D.; Williams, J. M.; Whitworth, J. R. Synth. Met. **1988**, *27*, A195.

[3]Sleight, A. W. Science 1988, 242, 1519.

[4](a) Holczer, K.; Klein, O.; Huang, S.-M.; Kaner, R. B.; Fu, K.-J.; Whetten, R. L.; Diederich, F. *Science*, **1991**, *252*, 1154. (b) Stephens, P. W.; Mihaly, L.; Lee, P. L.; Whetten, R. L.; Huang, S. M.; Kaner, R.; Deiderich, F.; Holczer, K. *Nature*, **1991**, *351*, 632.

[5](a) Binnig, G.; Rohrer, H.; Gerber, Ch.; Weibel, E.; *Phys. Rev. Lett.* **1982**, *49*, 57. (b) Spong, J. K.; Mizes, H. A.; LaComb, L. J.; Dovek, M. M.; Frommer, J. E.; Foster, J. S. *Nature*, **1989**, *338*, 137. (c) Smith, D. P. E.; Horber, H.; Gerber, Ch.; Binnig, G. *Science*, **1989**, *245*, 43.

[6]Binnig, G.; Quate, C. F.; Gerber, Ch. *Phys. Rev. Lett.* **1986**, *56*, 930.

[7](a) Tersoff, J.; Hamann, D. R. *Phys. Rev. B* **1985**, *31*, 805-813. (b) Tersoff, J. *Phys. Rev. Lett.* **1986**, *57*, 440.

[8](a) Tekman, E.; Cirai, S. *Phys. Rev. B* **1989**, *40*, 10 286. (b) Tromp, R. M. *J. Phys. Cond. Matter* **1989**, *1*, 10 211.

[9](a) Slater, J. C.; Koster, G. F. *Phys. Rev.* **1954**, *94*, 1498. (b) Bloch, F. *Z. Phys.* **1928**, *52*, 555. (c) Epstein, A. J.; Miller, J. S. Prog. Inorg. Chem. **198X**, *20*, 1. (d) Garito, A. F.; Heeger, A. J. *Acc. Chem. Res.* **1974**, *7*, 232-240.

[10] Bechgaard, K.; Jacobsen, C. S.; Mortensen, K.; Pedersen, H. J.; Thorup, N. *Solid State Commun.* **1980**, *33*, 1119-1125.

[11] Bechgaard, K.; Caneiro, K.; Rasmussen, F. B.; Olsen, M.; Rindorf, G.; Jacobsen, C. S.; Pedersen, H. J.; Scott, J. C. *J. Am. Chem. Soc.* **1981**, *103*, 2440-2442.

[12] Jacobsen, C. S.; Pedersen, H. J.; Mortensen, K.; Rindorf, G.; Thorup, N.; Torrance, J. B.; Bechgaard, K. *J. Phys. C.* **1982**, *15*, 2651-2663.

[13]Parkin, S. S. P.; Jerome, D.; Bechgaard, K. 1982, 79, 213-224.

[14]Mortensen, K.; Tomkiewicz, Y.; Schultz, T. D.; Engler, E. M. Phys. Rev. Lett. **1981**, *46*, 1234.

[15]Jerome, D.; Mazaud, A.; Ribault, M.; Bechgaard, K. J. Phys. Lett. **1980**, *41*, L95.

[16]Rindorf, G.; Soling, H.; Thorup, N. *Acta. Cryst.* **1982**, *B38*, 2805-2808.

[17](a) Lieber, C. M.; Wu, X. L. *Acc. Chem. Res.* **1991**, *24*, 170-177. (b) Parkinson, B. A. *J. Amer. Chem. Soc.* **1991**, *113*, 7833-7837.

[18](a) Wu, X. L.; Lieber, C. M.; Ginley, D. S.; Baughman, R. *J. Appl. Phys. Lett.* **1989**, *55*, 2129. (b) Parks, D. C.; Wang, J.; Clark, N. A.; Hermann, A. M. *Appl. Phys. Lett.* **1991**, *59*, 1506.

[19](a) Bai, C.; Dai, C.; Zhu, C.; Chen, Z.; Huang, G.; Wu, X.; Zhu, D.; Baldeschwieler, J. D. *J. Vac. Sci. Technol. A* **1990**, *8*, 484-487. (b) Yoshimura, M.; Shigekawa, H.; Nejoh, H.; Saito, G.; Saito, Y.; Kawazu, A. *Phys. Rev. B*, **1991**, *43*, 13590-13593. (c) Bando, H.; Kashiwaya, S.; Tokumoto, H.; Anzai, H.; Kinoshita, N.; Kajimura, H. *J. Vac. Sci. Technol.* **1990**, *A8*, 479-483. (d) Yoshimura, M.; Ara, N.; Kageshima, M.; Shiota, R.; Kawazu, A.; Shigekawa, H.; Saito, Y.; Oshima, M.; Mori, H.; Yamochi, H.; Saito, G. *Surface Science* **1991**, *242*, 18-22.

[20]Sleator, T.; Tycko, R. *Phys. Rev. Lett.* **1988**, *60*, 1418.

[21](a) Magonov, S. N.; Schuchhardt, J.; Kempf, S.; Keller, E.; Cantow, H.-J. *Synth. Met.* **1991**, *40*, 59-72. (b) Magonov, S. N.; Kempf, S.; Rotter, H.; Cantow, H.-J. *Synth. Met.* **1991**, *40*, 73-86.

[22](a) Blonder, G. E.; Tinkham, M. *Phys. Rev. B*, **1983**, *27*, 112. (b) van Bentum, P. J. M.; van Kempen, H.; van de Leemput, L. E. C.; Teunissen, P. A. A.; *Phys. Rev. Lett.* **1988**, *60*, 369-372.

[23](a) Nowack, A.; Weger, M.; Schweitzer, D.; Keller, H. J. *Solid State Commun.* **1986**, *60*, 199-202. (b) Hawley, M. E.; Gray, K. E.; Terris, B. D.; Wang, H. H.; Carlson, K. D.; Williams, J. M. *Phys. Rev. Lett.***1986**, *57*, 629-632. (c) Maruyama, Y.; Inabe, T.; Yamochi, H.; Saito, G. *Solid State Commun.* **1988**, *67*, 35-37. (d) Nowack, A.; Poppe, U.; Weger, M.; Schweitzer, D.; Schwenk, H. *Z. Phys. B.* **1987**, *68*, 41-47. (e) Maruyama, Y.; Hirose, R.; Saito, G.; Inokuchi, H. *Solid State Commun.* **1983**, *47*, 273-274. (f) Bando, H.; Kajimura, K.; Anzai, H.; Ishiguro, T.; Saito, G. *Proc. Seventeenth International Conference on Low-Temperature Physics*, Ecken, U.; Schmid, A.; Weber, W.; Wuhl, H., Eds.; North-Holland, Amsterdam, **1984**, p713-714. (g) More, C.; Roger, G.; Sorbier, J. P.; Jerome, D.; Ribault, M.; Bechgaard, K. *J. Phys. Lett. (Paris)* **1981**, *42*, L313-L317.

[24](a) Fainchtein, R.; Murphy, J. C. *J. Vac. Sci. Technol. B*, **1991**, *9*, 1013. (b) Pan, S.; Delozanne, A. L.; Fainchtein, R. *Journal of Vacuum Science & Technology B* **1991**, *9*, 1017-1021.

[25]Bondi, A. *J. Phys. Chem.* **1964**, *68*, 441.

[26](a) Flandrois, S.; Coulon, C.; Delhaes, P.; Chasseau, D.; Hauer, C.; Gaultier, J.; Fabre, J. M.; Giral, L. *Mol. Cryst. Liq. Cryst.* **1982**, *79*, 307-318. (b) Miller, J. S.; Epstein, A. J. *Prog. Inorg. Chem.* **1976**, *20*, 1.

[27]Uncertainties in the lattice constants determined by STM represent 2σ.

[28]The Se-Se contacts project slightly onto the [001] direction, and therefore the Se-Se interactions are not rigously along the [110] and [010] directions. We ignore the projection along the [001] direction, however, in order to simply the discussion.

[29]Wudl, F.; Shalom, E. A. J. Amer. Chem. Soc. 1982, 104, 1154.

[30]Jacobsen, C. S.; Tanner, D. B.; Bechgaard, K. *Phys. Rev. Lett.* **1981**, *46*, 1142.

[31](a) Kobayashi, H.; Kobayashi, A. *Extended Linear Chain Compounds*, Vol 2, **1982**, Miller, J. S., Ed.; Plenum Press, New York; p 275. (b) Friedel, J. Electron-Phonon Interactions and Phase Transitions, Vol 29, 1977; Riste, T., Ed.; Plenum Press, New York, pp. 1-49. (c) Kagoshima, S. *Extended Linear Chain Compounds*, Vol 2, **1982**, Miller, J. S., Ed.; Plenum Press, New York; p 311.

[32]Pouget, J. P.; Moret, R.; Comes, R.; Bechgaard, K.; Fabre, J. M.; Giral, L. *Mol. Cryst. Liq. Cryst.* **1982**, *79*, 129-143.

[33](a) Williams, J. M.; Keefer, K. D.; Washecheck, D. M.; Enright, N. P. Inorg. Chem. 1976, 15, 2446. (b) Reis, A. H. Jr.; Peterson, S. W.; Washecheck, D. M.; Miller, J. S. Inorg. Chem. 1976, 15, 2455-2462.

[34]Shaik, S. S.; Whangbo, M.-H. Inorg. Chem. 1986, 25, 1201.

[35]This charge localization can be described in molecular terms by considering the spatial relationship of the TMTSF molecules and the anions. In order to minimize Madelung energy, the anion beneath the surface layer of TMTSF molecules will tend to stabilize a net positive charge. These local state would therefore more closely resemble $TMTSF^+$ sites (with a nominal 1+ charge per molecule) which will have available empty states into which electrons can tunnel. Conversely, nominally neutral TMTSF sites without anions will more closely resemble neutral, closed-shell TMTSF molecules, which would not have available states for electron tunneling. In this case, reversing the polarity of the tunneling current should reveal the differences between these states.

[36](a) Whangbo, M.-H.; Williams, J. M.; Leung, P. C. W.; Beno, M. A.; Emge, T. J.; Wang, H. H.; Carlson, K. D.; Crabtree, G. W. *J. Amer. Chem. Soc.* **1985**, *107*, 5815. (b) Emge, T. J.;

Leung, P. C. W.; Beno, M. A.; Wang, H. H.; Firestone, M. A.; Webb, K. S.; Carlson, K. D.; Williams, J. M. *Mol. Cryst. Liq. Cryst.* **1986**, *132*, 363.

[37]Peierls, R. E. *Quantum theory of solids*, Clarendon, Oxford, **1965**. (c) Williams, J. M.; Wang, H. H.; Emge, T. J.; Geiser, U.; Beno, M. A.; Leung, P. C. W.; Carlson, K. D.; Thorn, R. J.; Schultz, A. J.; Whangbo, M.-H. Prog. *Inorg. Chem.* **1987**, *35*, 51.

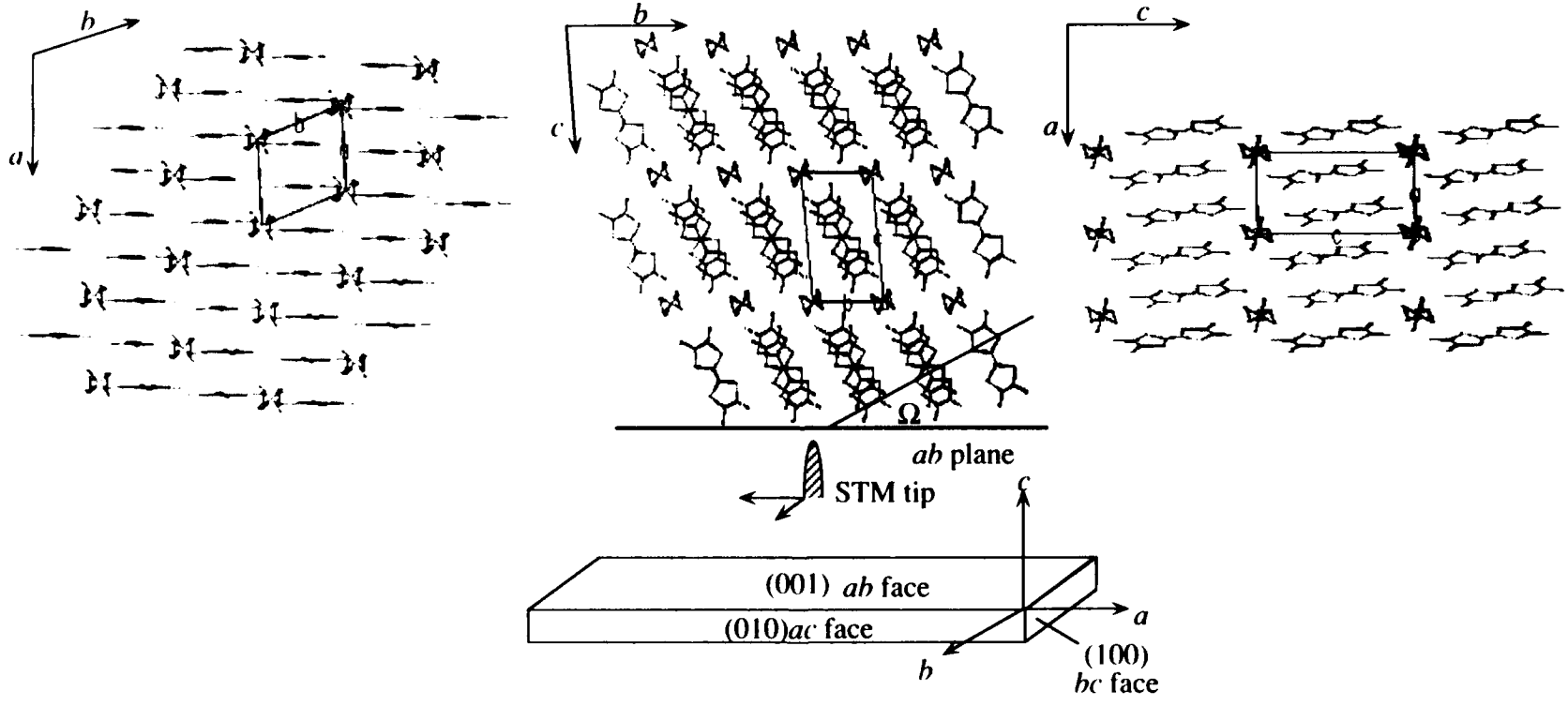
b
a
b
c
Ω
ab plane
STM tip
c
(001) ab face
(010)ac face
a
b
(100)
bc face
c
a

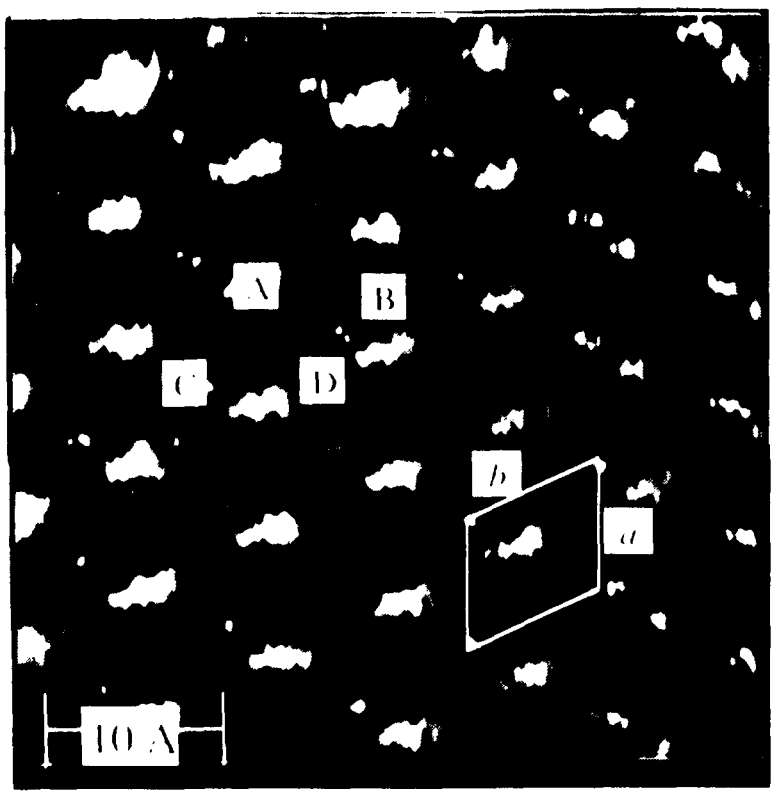

(a)

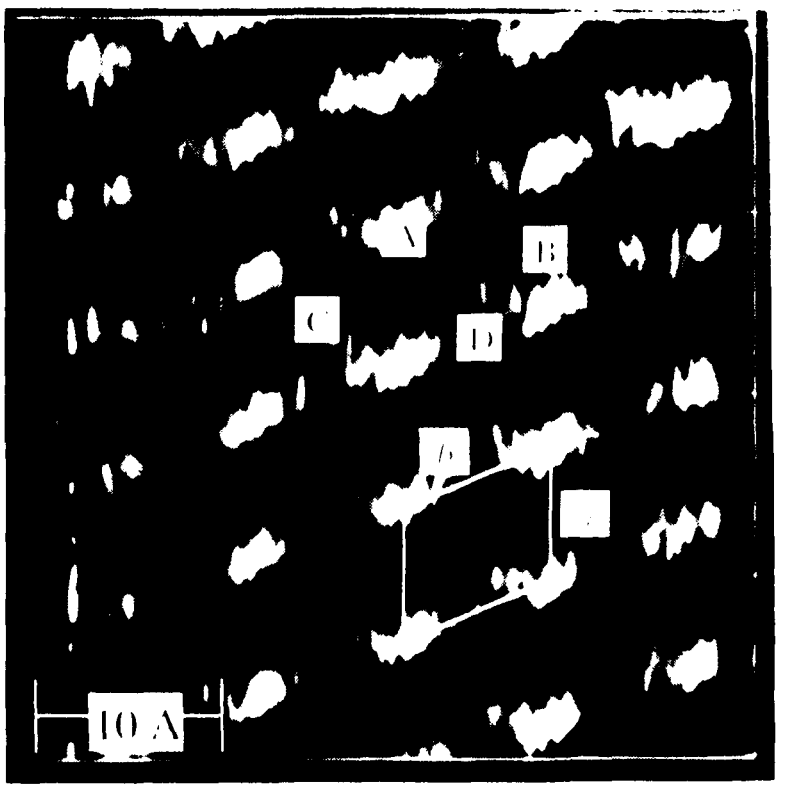

(b)

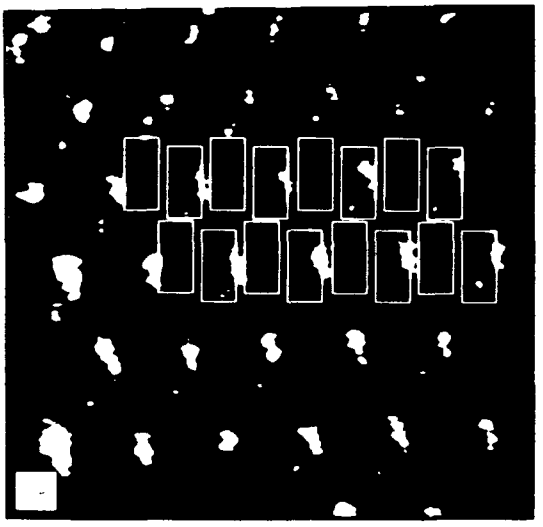
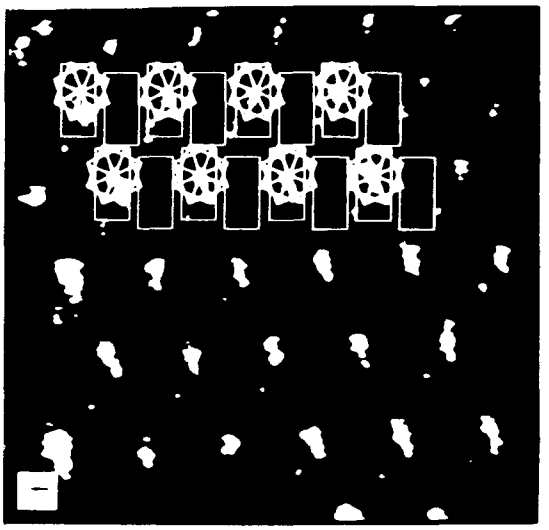
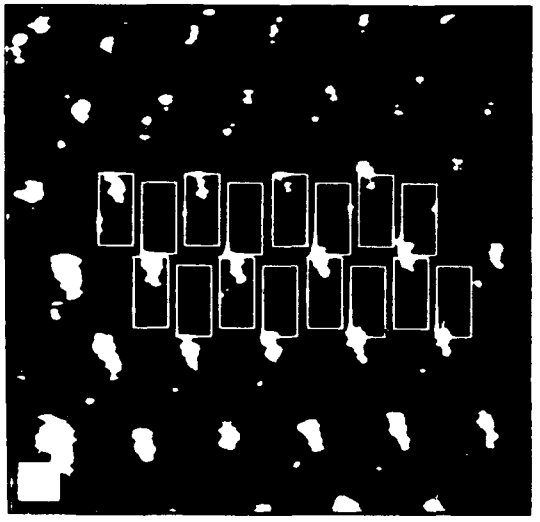
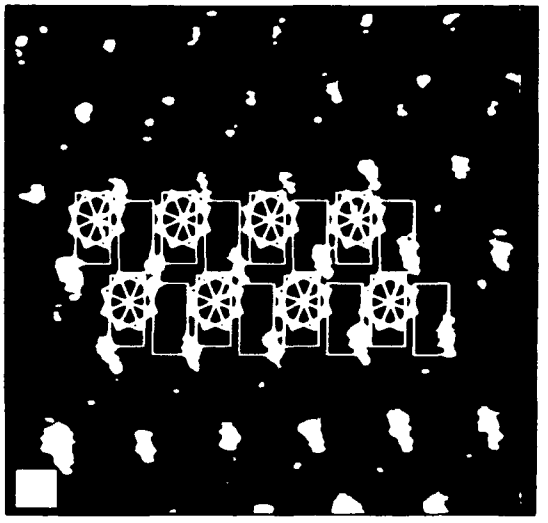
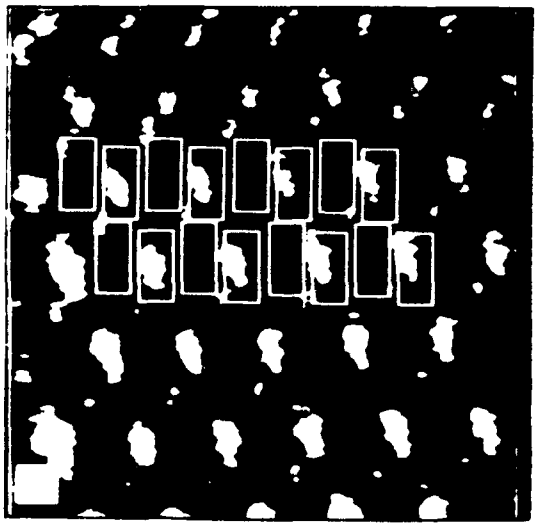
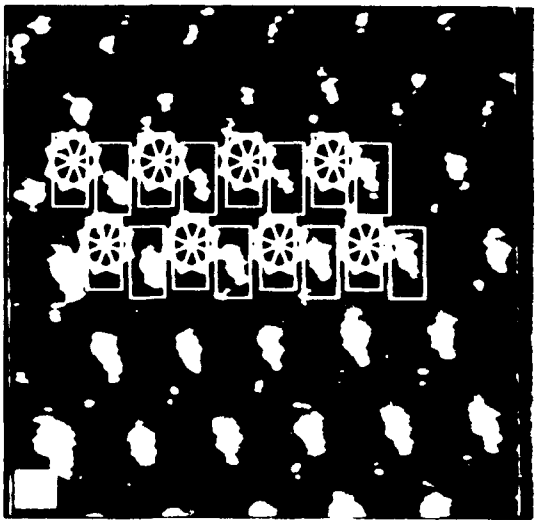

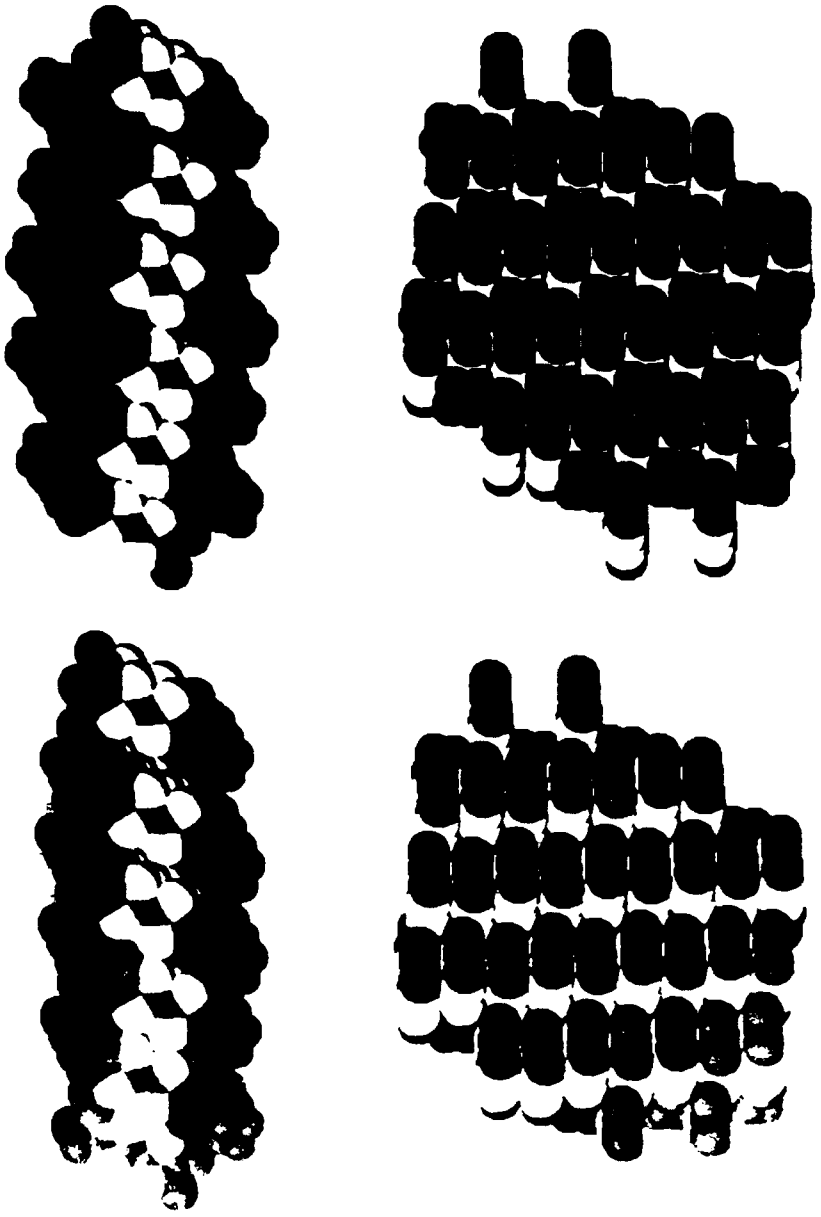

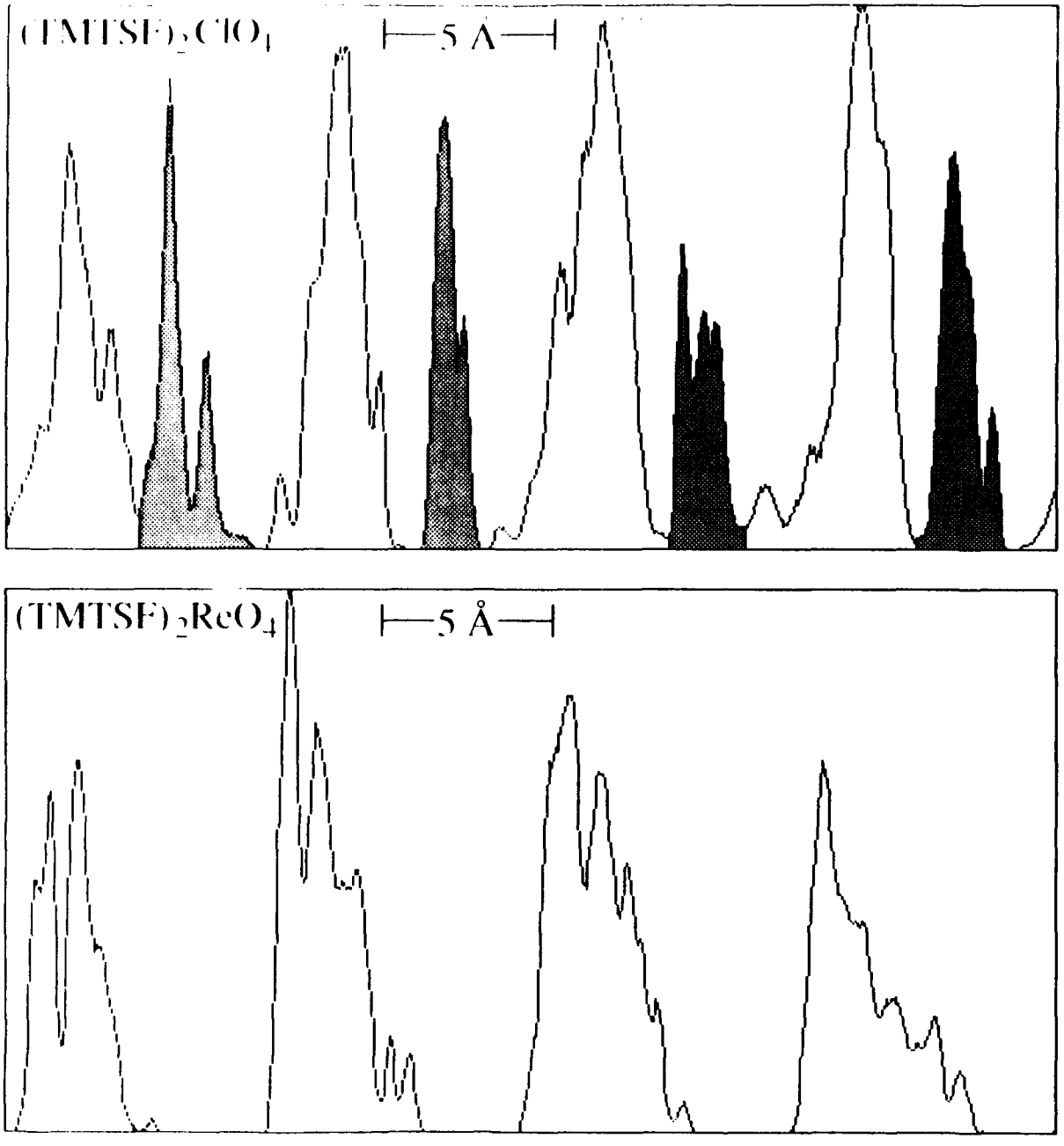
(TMTSF)2ClO4
5 Å
(TMTSF)2ReO4
5 Å